Binding-Linked Protonation of a DNA Minor-Groove Agent

Binh Nguyen,* Jaroslav Stanek,† and W. David Wilson*
*Department of Chemistry, Georgia State University, Atlanta, Georgia; and †Novartis Pharma AG, Basel, Switzerland

ABSTRACT The energetics for binding of a diphenyl diamidine antitrypanosomal agent CGP 40215A to DNA have been studied by spectroscopy, isothermal titration calorimetry, and surface plasmon resonance biosensor methods. Both amidines are positively charged under experimental conditions, but the linking group for the two phenyl amidines has a pK_a of 6.3 that is susceptible to a protonation process. Spectroscopic studies indicate an increase of 2.7 pK_a units in the linking group when the compound binds to an A/T minor-groove site. Calorimetric titrations in different buffers and pH conditions support the proton-linkage process and are in a good agreement with spectroscopic titrations. The two methods established a proton-uptake profile as a function of pH. The exothermic enthalpy of complex formation varies with different pH conditions. The observed binding enthalpy increases as a function of temperature indicating a negative heat capacity change that is typical for DNA minor-groove binders. Solvent accessible surface area calculations suggest that surface burial accounts for about one-half of the observed intrinsic negative heat capacity change. Biosensor and calorimetric experiments indicate that the binding affinities vary with pH values and salt concentrations due to protonation and electrostatic interactions. The surface plasmon resonance binding studies indicate that the charge density per phosphate in DNA hairpins is smaller than that in polymers. Energetic contributions from different factors were also estimated for the ligand/DNA complex.

INTRODUCTION

Proton uptake or release is often found in biological systems where protonation or deprotonation processes occur upon interactions or folding (1,2). With proteins, for example, a number of trypsin/thrombin inhibitors have been found to be protonated upon binding (3), and the protonation of cytosine-rich DNA sequences is observed upon folding into an i-motif (4). A typical example for small molecule-nucleic acid systems is the protonation of aminoglycosides on interaction with the RNA major groove (5–8). A number of DNA intercalators also have proton linkages to binding interactions (9,10). Consequently, the thermal stability of these structures or complexes is highly pH-dependent, and their binding affinities vary with proton activity. For nucleic acid systems, theoretical treatments have led to the proposal that the DNA minor-groove environment is more acidic than its surroundings (11). Experimental probing of the minor groove with carboxylic groups in mixed sequences has confirmed the calculated results (12). This acidic environment presumably plays a critical role in protonation of ligands with basic groups that have pK values in an appropriate range. It is interesting, however, that there has been no detailed study of a binding-linked protonation of a minor-groove binding agent.

The compound CGP 40215A (Fig. 1) (13) has four unique properties distinguishing it from other DNA binding agents. First, it has been found to have biological activity against a number of parasitic microorganisms (14,15). Second, although CGP 40215A lacks the curvature usually seen with DNA minor-groove binders, DNA interaction studies indicate a high binding affinity with AT-rich sequences. A wide range of biophysical techniques including DNase I footprinting, ultraviolet-visible spectroscopy, circular and linear dichroism, surface plasmon resonance, x-ray crystallography, and molecular dynamics simulations have illustrated that CGP 40215A binds strongly to AT-rich sequences of DNA duplexes in the minor groove (16–18). Third, x-ray structural results show that a bound water molecule is involved in H-bond interactions between an amidinium of the compound and DNA. Fourth, preliminary studies have also shown partial protonation of the ligand near physiological pH. This ligand/DNA complex thus represents a unique system for investigation of both protonation-linked processes and the influence of a directly bound water molecule in minor-groove complex formation. Here, the proton linkage (uptake) to the binding at equilibrium is studied in detail using absorption spectral pH titration and isothermal titration calorimetry (ITC). The energetics of electrostatic interactions in complex formation are also characterized by measuring the binding affinities under different salt concentrations using surface plasmon resonance.

MATERIALS AND METHODS

Absorption spectral titrations

CGP 40215A was synthesized as previously described (13) and used with an extinction coefficient $\varepsilon_{327} = 25{,}300\ cm^{-1}\ M^{-1}$ (water, room temperature). Because the maximum absorption wavelength varies with the solution pH, the extinction coefficient at an isobestic wavelength (327 nm) was used. The DNA concentration was determined using the nearest-neighbor method (19–21). For pK_a determinations, the compound was dissolved in 0.1 M NaCl in a 3-mL cell (5.8 μM) and titrated with NaOH solution. Concentrated HCl solution was used to make the solution near pH 3 at the beginning. For bound pK_a determination the complex solution (2.3×10^{-8} mol compound

Submitted July 26, 2005, and accepted for publication November 1, 2005.

Address reprint requests to W. David Wilson, Dept. of Chemistry, Georgia State University, University Plaza, Atlanta, GA 30303. Tel.: 404-651-3903; Fax: 404-651-1416; E-mail: wdw@gsu.edu.

0006-3495/06/02/1319/10 $2.00

doi: 10.1529/biophysj.105.071381

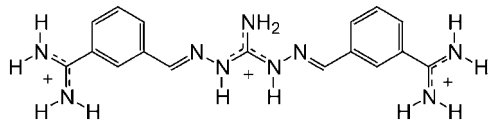

FIGURE 1 Structure of CGP 40215A.

and 4.6×10^{-8} mol duplex d(GCGAATTCGC)$_2$) in 0.1 M NaCl was titrated with NaOH solution in a similar manner. The normalized absorbance changes, Y (the fraction of unprotonated linker), as a function of pH values were fitted with a derived form of the Henderson-Hasselbalch equation to obtain pK_a values of the free and bound ligand:

$$Y = [10^{(\mathrm{pH}-\mathrm{pKa})}]/[1 + (10^{(\mathrm{pH}-\mathrm{pKa})})]. \quad (1)$$

The fraction of protons, n_{abs}, linked over this range of pH can be described as

$$n_{abs} = Y_{free} - Y_{bound}, \quad (2)$$

where Y_{free} is the fitted titration curve of free ligand and Y_{bound} that of bound ligand.

Isothermal titration calorimetry

Calorimetric experiments were performed with a VP-ITC (MicroCal, Northampton, MA). The instrument was electrically calibrated with heat pulses and chemically calibrated by titration with the following pairs of reagents: RNase A/2′CMP, $BaCl_2$/18-Crown-6, and HCl/THAM, as described previously (22). Within experimental error, the obtained values are in agreement with literature values (23–25).

To evaluate the linked protonation equilibrium, calorimetric experiments were conducted at 25°C in two pairs of buffers at two different pHs. The buffer solutions include cacodylate buffer (0.01 M cacodylic acid, 0.1 M NaCl, 0.001 M EDTA, pH 6.25), MES buffer (0.01 M [2-(*N*-morpholino)ethanesulfonic acid, 0.1 M NaCl, and 0.001 M EDTA, pH 6.25), TES buffer (0.01 M *N*-tris(hydroxymethyl) methyl-2-aminoethanesulfonic acid, 0.1 M NaCl, and 0.001 M EDTA, pH 7.45), HEPES buffer (0.01 M *N*-(2-hydroxyethyl)piperazine-*N*′-(2-ethanesulfonic acid), 0.1 M NaCl, and 0.001 M EDTA, pH 7.45). These pairs of buffers have close pK_a values yet different heats of ionization. The heats of ionization of the buffers are from the results of Fukada and Takahashi (MES, 3.712 kcal/mol; cacodylate, −0.468 kcal/mol; TES, 7.825 kcal/mol; HEPES, 5.022 kcal/mol) (26).

The DNA polymer poly(dAdT)·poly(dAdT) (0.12 mM basepairs) was calorimetrically titrated with 3-μL injections of 0.47 mM CGP 40215A at 25°C in MES buffer. Blank titrations were conducted by injecting the ligand into the buffers under the same conditions. The corrected heat profile was obtained by subtracting the blank titration heat from the raw heat and the corrected result was fitted using the Origin software provided with the instrument (Origin, version 5.0, MicroCal).

The observed enthalpy change per mol of complex formation can be expressed as

$$\Delta H_{obs} = \Delta H_{int} + n_{cal}(\Delta H_{Lp} + \Delta H_i), \quad (3)$$

where ΔH_{int} is the intrinsic heat of binding of the fully protonated ligand; n_{cal} is the number of mol of linked protons determined calorimetrically; ΔH_{Lp} is the heat of ligand protonation; and ΔH_i is the heat of dissociation of the protonated buffer

For a system of two buffers (b1 and b2) at the same pH, the number of mols of protons linked per mol of complex formation can be evaluated as

$$n_{cal} = (\Delta H_{obs}\mathrm{b1} - \Delta H_{obs}\mathrm{b2})/(\Delta H_i\mathrm{b1} - \Delta H_i\mathrm{b2}). \quad (4)$$

Calorimetric titrations of the ligand into the AATT DNA hairpin, d(CGAATTCG**TCTC**CGAATTCG) (loop in bold) solution, were conducted at different temperatures to determine the heat capacity change. The DNA sample was heated before the titration above its T_m value and rapidly cooled down in ice to assure the hairpin species is dominant. The DNA (2 μM of hairpin) inside the cell was titrated with 5-μL injections of 0.05 mM ligand. Blank titrations were conducted in a similar manner without the DNA. It was observed that the heat of the blank titration is about −1 kcal/mol from 288 K to 318 K, pH 6.25. The blank titration heat was subtracted from the uncorrected CGP/DNA titration heat, and the data was fitted to a 1:1 binding model to obtain the free energy, binding enthalpy, and entropy.

Surface plasmon resonance (SPR) biosensor

The binding affinities of the ligand to DNA hairpins at different salt concentrations were determined using a BIACORE 3000 (Biacore, Uppsala, Sweden) instrument with SA chips. The DNA immobilization was conducted by manual injection of a 14-nM 5′biotinated DNA hairpin solution onto the desired flowcell at a flow rate of 1 μl/min. Typically, an amount of ~400 resonance units (RU) was immobilized on each flow cell. Three flow cells contained DNA and one was left blank for reference. The binding sensorgrams (in MES buffer at various salt amounts with 0.0005% P20 surfactant) were collected by injecting a series of ligand concentrations at a flow rate of 20 μl/min for a 10-min period followed by a 6-min dissociation time. A long injection time was used to obtain a steady-state plateau of sufficient data points to average. Steady-state methods lose kinetic information but eliminate any mass transport effects. The flow-cell surfaces were regenerated by multiple 1-min injections of a concentrated salt solution. The response in RU was normalized to fraction bound by dividing the averaged steady-state responses by the predicted maximum response, RU_{pred}, per bound ligand, as previously described (27). A plot of this normalized response, r, versus ligand concentration was generated and fitted with a one-site model. The ligand concentration in the flow is the free ligand concentration, C_{free}:

$$r = (K_a \times C_{free})/(1 + K_a \times C_{free}). \quad (5)$$

Heat capacity changes

The heat capacity change on complex formation can be predicted as described for protein systems (28) with protonation/deprotonation terms added.

$$\Delta Cp_{total} = \Delta Cp_{he} + \Delta Cp_v + \Delta Cp_{nc} + \Delta Cp_p + \Delta Cp_{dp} + \Delta Cp_{ot}, \quad (6)$$

where ΔCp_{he} is from hydrophobic effects associated with the burial of nonpolar areas. This term can be evaluated from calculating solvent accessible surface area change ($\Delta SASA$); thus, the term ΔCp_{he} is used interchangeably with ΔCp_{SASA}. The terms ΔCp_v and ΔCp_{nc} are, respectively, from internal vibrations/stretching of covalent bonds and from vibrations of noncovalent interactions. The term ΔCp_p is from protonation of ligand, and ΔCp_{dp} is from the deprotonation of buffer component. The heat capacity change that arises from secondary structure effect, ΔCp_{nc}, is small and evaluated as -0.0087 $(\Delta SASA)_{total}$ (29,31), and the contribution from the deprotonation of buffer, ΔCp_{dp}, is $n_H \Delta Cp_{buffer}$ (26), where n_H is the number of protons uptaken per mol of complex, and ΔCp_{buffer} is the heat capacity change of buffer deprotonation. The last term ΔCp_{ot} is from other factors such as ion-pair and bound water and surface water (32–36).

The heat capacity change associated with the burial of polar/nonpolar areas, ΔCp_{SASA}, was computed from the change in SASA of the CGP/DNA complex (Nucleic Acid Database id, DD0052; Protein Data Bank id, 1M6F) (37), free DNA duplexes, and the free ligand. The areas were calculated with a probe radius of 1.4 Å using GRASP (38) with the default radii or Cornell et al. radii with a probe radius of 1.7683 Å. (39) The structures were initially processed with SYBYL 6.9 (Tripos, St. Louis, MO). Water, ions, and other unknown atoms were removed, and hydrogen atoms were added. Carbon, carbon-bound hydrogen, and phosphorous atoms are designated as nonpolar atoms, and all others are polar. Consequently, the 12-mer DNA duplex

$(CGCGAATTCGCG)_2$ has 288 polar atoms and 470 nonpolar atoms, and the ligand has 21 polar atoms and 27 nonpolar atoms. The changes in SASA of the polar and nonpolar areas of the free DNA and free ligand were calculated as followed:

$$\Delta SASA = SASA_{\text{complex}} - (SASA_{\text{free-dna}} + SASA_{\text{free-ligand}}). \quad (7)$$

The $SASA_{\text{free-dna}}$ term was calculated using the DNA duplex from the complex with the ligand removed (17), from the average of five NMR structures (40), or from an x-ray structure of the duplex (41), The heat capacity change arising from the burial of polar (*A*p) and nonpolar areas (*A*np) upon binding is estimated using three different models and two different radii sets. The models were empirically derived from amide transfer/protein folding (Eq. 8) (42–45), from protein folding (Eq. 9) (29–31,46,47), or from a set of five DNA-intercalator complexes (Eq. 10) (48):

$$\Delta Cp_{\text{SASA}} = (0.32 \pm 0.04)\Delta A\text{np} - (0.14 \pm 0.04)\Delta A\text{p}; \quad (8)$$

$$\Delta Cp_{\text{SASA}} = (0.45 \pm 0.02)\Delta A\text{np} - (0.26 \pm 0.03)\Delta A\text{p} + (0.17 \pm 0.07)\Delta A_{\text{OH}}; \quad (9)$$

$$\Delta Cp_{\text{SASA}} = (0.382 \pm 0.026)\Delta A\text{np} - (0.121 \pm 0.077)\Delta A\text{p}. \quad (10)$$

The electrostatic contribution was estimated with (49)

$$\Delta G_{\text{elec}} = Z\varphi \times R \times T \times \ln[\text{Na}^+]; \quad \text{where}$$

$$(\delta \log(K_{\text{obs}})/\delta \log([a^+_{\text{Na}}])) = -Z\varphi, \quad (11)$$

where Z is the charge of the ligand, and φ is the fraction of Na^+ per phosphate.

RESULTS

Spectrophotometric titrations and pK_a values

The ultraviolet-visible pH titration spectra of free CGP 40215A and the CGP/d$(GCGAATTCGC)_2$ complex in 100 mM NaCl are shown in Fig. 2. Spectral changes upon addition of NaOH to an acidic solution of the compound or complex are similar to previous observations in water (18). Fitting the spectral changes from spectrophotometric pH titrations for free CGP 40215A and DNA-bound CGP 40215A in 100 mM NaCl yielded pK_a values of 6.3 ± 0.1 and 9.0 ± 0.1, respectively (Fig. 2), which indicates an increase of 2.7 pK_a units between the free and bound ligand under these conditions. Near the end of the titration (pH ~6.7), the free ligand appears to behave nonideally. The fit of the data with the last four data points removed, however, is insignificantly different from the fit when those points are included. The linked protonation profile (n) of the ligand can be described by the difference in the pH titration curves of free and bound ligand, which defines the difference in bound proton for free and DNA-bound CGP. The maximum proton uptake at $n = 0.92$ occurs at pH 7.7. Benzamidine groups are known to have pK_a values >10 (50,51) and are not significantly deprotonated in the pH range below 10 (Fig. 2). For pH titrations of the complex, excess DNA was added to a CGP concentration that was high enough to ensure the complete binding of the compound. Although the DNA *T*m is known to be decreased at very high or low pHs, the temperatures and the pH range in this study are below the *T*m. The ITC binding studies in acetate buffer confirm the binding at pH 5.00. At pH 10, it is expected that the binding affinity is reduced because of the compound linker deprotonation. Spectrophotometric titration spectra of the DNA into the ligand at pH 10 exhibit an isobestic point at 371 nm (see Supplemental Material, Fig. S2) and, based on the absorbance changes, indicate the complete binding of CGP under the pH titration conditions.

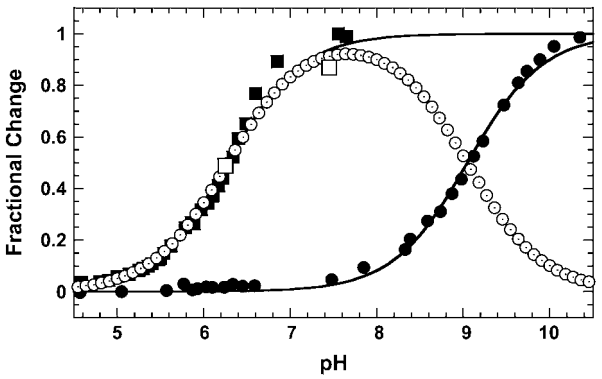

FIGURE 2 Fractional absorbance change of the free (■) and bound (●) ligand, and the fractional proton uptake (○). Solid lines are the fits using Eq. 1; the pK_a values are 6.3 ± 0.1 and 9.0 ± 0.1 for the free and bound ligands, respectively. Maximum proton uptake occurs at pH 7.7. Calorimetric titration results at two pH values (□) are also plotted, illustrating a good agreement.

Calorimetric titrations

Calorimetric titration curves of poly(dAdT) · poly(dAdT) with CGP 40215A at pH 6.25 (in cacodylate or MES buffer) are shown in Fig. 3. The corrected heat profile shows that the transition of the primary binding occurs at a compound/DNA_{basepair} ratio of around 0.12, equivalent to 1 compound per 8 base pairs. The observed enthalpy change is different in the two experiments and this is caused by the difference in ionization heats of the two buffers. It was observed that an enthalpy change arising from much weaker nonspecific binding is observable at higher ratios of compound to DNA in MES or cacodylate buffer (Fig. 3). Therefore, the results were fitted using the Origin 5.0 software with a sequential binding site model that accounts for the strong primary site and weak nonspecific sites. Similar titrations were conducted in TES or HEPES buffer at pH 7.45. It was found from the calorimetric titration results and Eq. 4 that the number of protons being taken up upon complex formation is 0.49 at pH 6.25 and 0.87 at pH 7.45. These values are consistent with those predicted from spectrophotometric titrations as shown in Fig. 2 and Table 1. From these values, the pK_a of bound ligand was calculated to be 8.9 ± 0.5 at pH 6.25 and 8.6 ± 0.5 at pH 7.45. Calorimetric methods were also used to

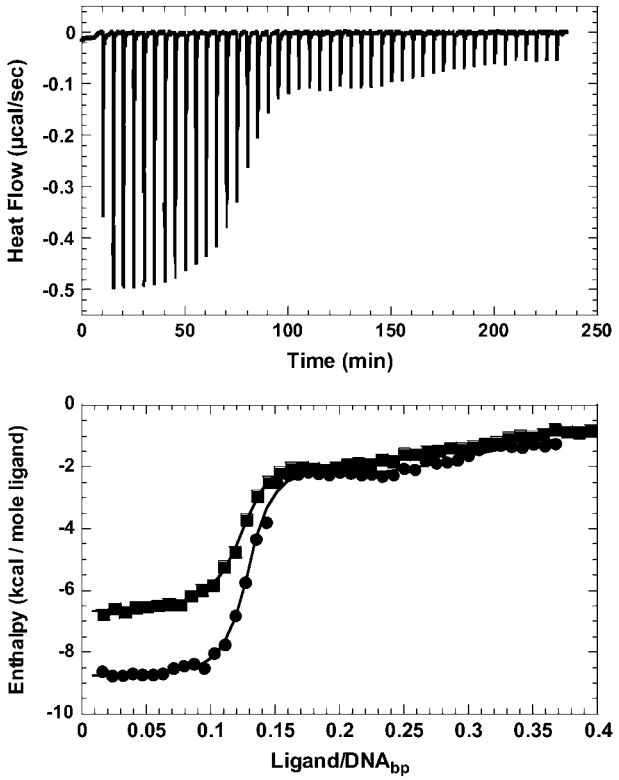

FIGURE 3 ITC titrations of CGP with poly(dAdT) · poly(dAdT) in MES and cacodylate buffers. Top panel is a representative titration curve of 3-μL injections of 0.473 mM CGP into 0.12 mM DNA base pairs in cacodylate buffer at pH 6.25, 25°C. Bottom panel is a plot of integrated heats per mol of CGP in cacodylate buffer (●) and in MES buffer (■) versus the ratio of the ligand to DNA base pairs. The primary binding occurs at a ratio of 0.125 that is equivalent to one compound per eight base pairs. It can be seen that 1), a significant difference in the heat release occurs at the primary binding between the two buffers under the same conditions; and 2), secondary binding to the polymer occurs at higher ratios in both buffers.

probe the effects of oligomer/polymer on the proton uptake. The consistency in fraction of proton uptake at two different pHs from two methods confirms that the protonation is the same on DNA oligomers as on DNA polymers. This similarity of the results also suggests that under these conditions experimental results with oligomers are not significantly influenced by end effects.

Isothermal titration of the DNA hairpin AATT with the ligand was conducted at various temperatures to obtain the CGP binding enthalpies as a function of temperature. It should be emphasized that the observed binding enthalpies include intrinsic binding enthalpy coupled with ligand protonation and the buffer deprotonation heat. A representative ITC curve at 298 K and a fit of its integrated areas are shown in Fig. 4. A plot of the observed enthalpy changes as a function of temperature is shown in Fig. 5. This plot can be fitted within experimental errors by a linear fit, suggesting that the heat capacity change is constant in this temperature range and equal to –155 ± 16 cal/(mol·K) at pH 6.25. Calorimetric titrations

TABLE 1 Summary of observed binding enthalpies in two different buffers at two different pH values

pH	ΔH_{obs} (kcal/mol) (buffer)	pK_a bound*	n_{cal}	n_{abs}	n_{cal}/n_{abs}
6.25	−8.77 (cacodylate) −6.73 (MES)	8.9 ± 0.5	0.49	0.49	1.0
7.45	−6.30 (TES) −8.74 (HEPES)	8.6 ± 0.5	0.87	0.91	0.95

The pK_a values and fractions of proton uptake (n) at two pH values from calorimetric and absorption spectrophotometric titrations are also shown. n_{cal}, fraction of protons uptake determined from calorimetric titrations using Eq. 4; n_{abs}, fraction of proton uptake determined from absorption spectroscopic titrations using Eq. 2.

*The calculated pK_a values of bound ligand using calorimetric results and pK_a. The pK_a values of the free and bound ligand obtained from fitting of spectroscopic data are 6.3 ± 0.1 and 9.0 ± 0.1, respectively.

were also conducted at a lower pH (acetate buffer, pH 5), where proton uptake upon binding is minimized. Linear fitting of the observed binding enthalpies as a function of temperature at the lower pH yields a larger negative slope, −234 ± 11 cal/(mol·K). (Fig. 5).

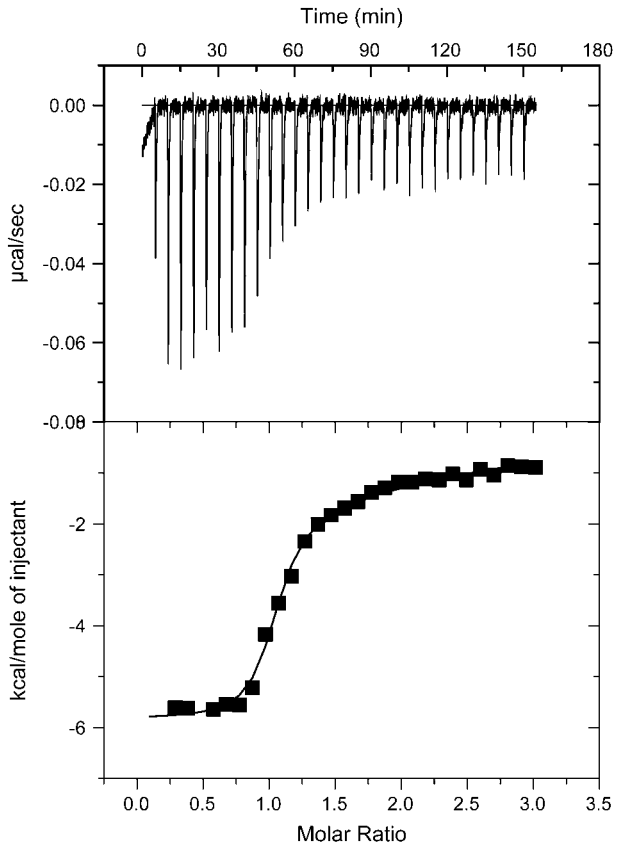

FIGURE 4 An isothermal calorimetric titration curve of CGP 40215A into AATT hairpin solution. Every peak represents the heat released from a 5-μl injection of 50 μM CGP into 2 μM oligomer concentration in MES buffer with 0.1 M NaCl, pH 6.25 at 298 K. The corrected heat was fitted to obtain thermodynamic binding parameters.

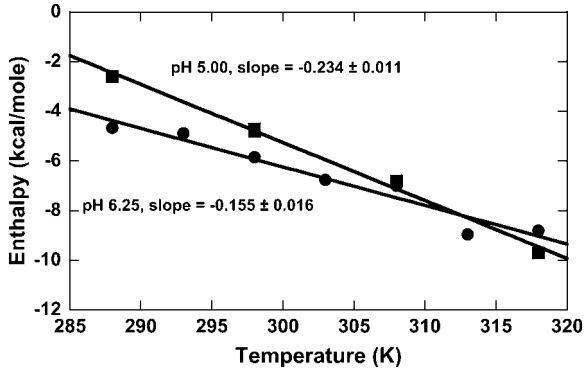

FIGURE 5 Effects of solution pH on the heat capacity change. In MES buffer (10 mM MES, 0.1 M NaCl, 1 mM EDTA, pH 6.25), linear fitting of the observed binding enthalpy as a function of temperature yields a slope of –155 ± 16 cal/(mol·K). The slope becomes more negative (−234 ± 11 cal/(mol·K)) in acetate buffer (10 mM acetate, 0.1 M NaCl, 1 mM EDTA, pH 5.00), where proton linkage is minimized.

SPR biosensor and affinities

The binding constants under various salt concentrations and pHs were also determined by SPR with an immobilized DNA hairpin. Typical sensorgrams for the interaction of CGP 40215A with the AATT binding site in HEPES buffer (pH 7.45) are shown in Fig. 6 together with a fitting plot. As expected from electrostatic competition, the binding affinity is decreased at higher salt concentrations. The binding constant drops ~3.4 times when the salt concentration is doubled. Based on the polyelectrolyte theory (49,52), the number of counterions released and the electrostatic contribution to the observed binding free energies can be estimated. The binding constants at various salt concentrations and two different pH conditions are plotted and linearly fitted in Fig. 7. The slopes, $-Z\phi$, are -2.1 ± 0.1 at pH 6.25 and -2.0 ± 0.2 at pH 7.45. Under the same salt concentrations, the binding affinities are reduced at higher pHs, supporting a linked-protonation equilibrium. The counterion density per phosphate is $\phi = 0.88$ for DNA B-form polymer (49,52). Since an AATT binding site is in the central region of the DNA, we assume this value is a good approximation, and the counterion release values, Z, were calculated to be 2.4 and 2.3 at pH 6.25 and 7.45, respectively. These values are higher than that of a dication, confirming an additional charge of the ligand upon complex formation. The free energy from electrostatic interactions, ΔG_{elec}, is computed using Eq. 11. At pH 6.25, 298 K, and 0.1 M NaCl, the electrostatic component contributes about –2.9 kcal/mol to the total binding energetics. As expected, this electrostatic contribution becomes smaller at higher salt concentrations, and the reduction of this component contributes to reduced binding affinities at high salt concentrations. The SPR experiments were not conducted at salt concentrations <50 mM to minimize the possible electrostatic interaction between the positively charged ligand and the flow-cell surface.

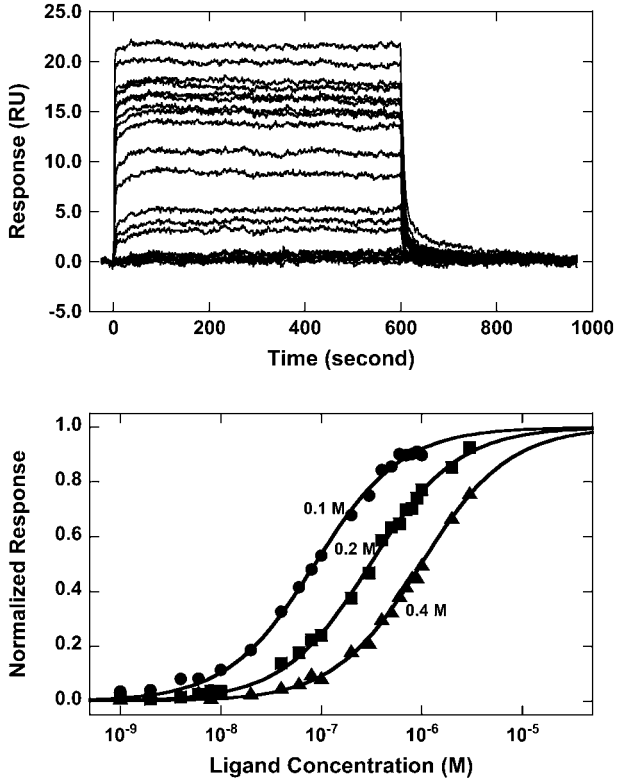

FIGURE 6 SPR binding affinities. Top panel is a plot of sensorgrams for the interaction of CGP with 5′biotin-CGAATTCGTCTCCGAATTCG-3′ hairpins in HEPES buffer at pH 7.45, 0.2 M NaCl, and 25°C. Bottom panel is a plot of stoichiometry-normalized binding isotherms at three different NaCl concentrations: 0.1 M, 0.2 M, and 0.4 M.

SASA and heat capacity change

Although a number of factors can influence the heat capacity change on complex formation, a relationship between the solvent-accessible surface area change and the heat capacity change has been derived for diverse processes. For DNA

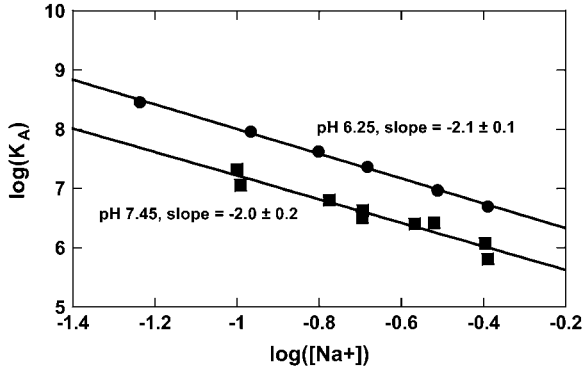

FIGURE 7 Binding affinities at different salt concentrations and two different pHs. The dependence of free energies on salt concentrations at pH 6.25 and pH 7.45. The slopes are −2.1 at pH 6.25 and −2.0 at pH 7.45. Using these slopes and the ligand charges, the counterion density per phosphate at the binding site is 0.68 ± 0.02.

interactions, the prediction is based on the area change (polar and nonpolar) between the complex and free DNA and free ligand. The surface area of free DNA was calculated from the NMR solution structure of a 12-mer AATT duplex (40), the x-ray structure of DNA duplex alone (41), or the DNA extracted from the complex (17). For comparison, two different sets of radii were used: the default set in GRASP (38) and the Cornell et al. radii (39). Traditionally, a water probe radius of 1.4 Å is used in calculations of SASA. To be consistent with use of the Cornell radii, a probe radius of 1.7683 Å is used. This radii set has been widely used in molecular dynamic simulations of nucleic acids, yielding successful results (53–55). Although the total areas are compatible for two methods, the computed nonpolar areas using GRASP radii are consistently lower than those using Cornell et al. radii (Table 2 and Supplementary Material, Table S2). This is the result of different radii assignments. Calculations with the Cornell et al. radii yield heat capacity change values that are close to the experimental values. The calculated results using GRASP radii are available in Supplementary Material. The results of the polar and nonpolar areas of the DNA and its complex with the ligand using the Cornell et al. radii are summarized in Table 2, and an illustration of solvent-accessible surface area of the whole complex is shown in Fig. 8. As seen in this figure, the ligand is deeply submerged within the minor groove of the DNA and largely shielded from the solvent, despite its relatively linear shape. The areas of the free unbound DNA extracted from the complex are within the error of the average from five NMR structures. The SASA results from NMR structures or the DNA extracted from the complex indicate that >80% of the total area of the ligand is buried when it binds to DNA (nearly equal contributions of polar and nonpolar components: 52% and 48%, respectively). Only ~4–5% of total DNA area is buried and >80% of this total comes from the nonpolar component (see Table 2). As shown in Table 2, the results obtained from the free DNA x-ray structure are smaller than those obtained from unbound DNA or NMR structures. This suggests that the x-ray structure is somewhat compact relative to the solution structure in terms of SASA. Although its polar area is in agreement with the unbound or NMR structures, its nonpolar area is remarkably reduced. The predicted hydrophobic contribution to the heat capacity change was evaluated using empirical derived relations (Eqs. 8–10). A summary of the results using three different equations and different DNAs is shown in Table 3.

TABLE 2 Calculations of solvent-accessible surface area (Å^2)

	Polar area (A_p)	Nonpolar area (A_{np})	Total area
Complex	2747	2045	4792
Bound DNA	2693	1951	4643
Bound ligand	54	95	149
Unbound ligand	361	414	774
Unbound DNA*	2740	2135	4875
Free NMR DNA†	2707 ±31	2143 ± 87	4851 ± 77
X-ray structure‡	2705	2008	4714
	$\Delta A^* = -354$	$\Delta A^* = -503$	$\Delta A^* = -858$
	$\Delta A^\dagger = -321$	$\Delta A^\dagger = -512$	$\Delta A^\dagger = -833$
	$\Delta A^\ddagger = -319$	$\Delta A^\ddagger = -377$	$\Delta A^\ddagger = -696$

SASA values were found using GRASP (38) with Cornell et al. radii with a probe radius of 1.7683 Å (39).
*The DNA structure is extracted from the complex (17).
†The average of five NMR structures (40).
‡The DNA structure is from x-ray experiments in NaCl (41).

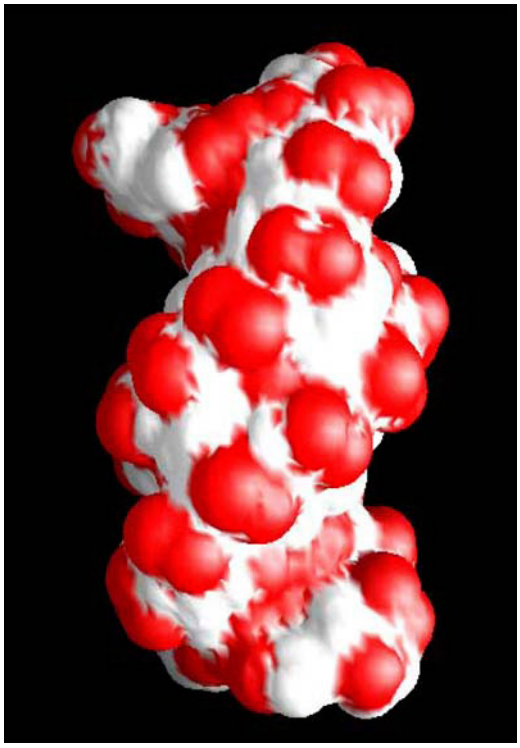

FIGURE 8 Solvent-accessible surface area of the complex generated by the GRASP program. A view is at the minor groove with the ligand bound at the AATT site. The polar atoms are in red and nonpolar atoms are in white. Arrays of polar phosphate-bound oxygen atoms are visible along the DNA backbone. The red areas in the minor groove are the nitrogen, and nitrogen-bound hydrogen atoms of the ligand. The accessible surface was generated using Cornell et al radii (39) with a probe radius of 1.7683 Å.

Enthalpy and heat capacity change

A profile of the observed enthalpy changes as a function of pH value (from 5 to 7) was obtained by conducting the titrations in a buffer solution consisting of MES ($pK_a = 6.2$) and TES ($pK_a = 7.5$) (Supplementary Material, Fig. S1). The observed heats vary with pH, as expected. At 298 K, as pH increases, the observed enthalpy change varies significantly, indicating the linkage between the heat of protonation of the ligand and deprotonation of the MES buffer. At pH 5, the free ligand is almost fully protonated (no uptake occurs upon binding); the observed value is the intrinsic enthalpy, −5 kcal/mol. This value is consistent with the result in acetate buffer at pH 5. At pH 6.25 in MES buffer, the observed

TABLE 3 Heat capacity change (cal/(mol·K)) from SASA change for the interaction of CGP with the AATT site

	Eq. 8 (44)	$\Delta Cp_{he}/\Delta Cp_{obs}$	Eq. 9 (29)	$\Delta Cp_{he}/\Delta Cp_{obs}$	Eq. 10 (48)	$\Delta Cp_{he}/\Delta Cp_{obs}$
Unbound DNA	−111 ± 34	0.47	−134 ± 21	0.57	−149 ± 40	0.64
NMR	−119 ± 33	0.51	−147 ± 20	0.63	−157 ± 38	0.67
X-ray	−76 ± 28	0.32	−87 ± 17	0.37	−105 ± 34	0.45

The calculated values were obtained from the Cornell et al. radii (39) using Eqs. 8–10 and three different DNA duplex structures of the same sequence from NMR or x-ray experiments (see text and Table 2). The ratios of the calculated hydrophobic heat capacity change to the experimentally observed value at pH 5.00 (−234 ± 11 cal/(mol·K)) are also shown.

enthalpy is −5.8 kcal/mol as shown in Fig. 5. Thus, a difference of −0.8 kcal/mol includes the heat of protonation of ligand and deprotonation of MES. Under these conditions, there is ~0.5 mol of MES buffer deprotonation and 0.5 mol ligand protonation. The heat of deprotonation of MES buffer is ~3.7 kcal/mol (26). Thus, for one mol of complex, 1.85 kcal/mol of heat comes from MES deprotonation and, therefore, a net heat of −2.65 kcal/mol comes from ligand protonation. In other words, the heat of protonation of ligand linker, $\Delta H_{Lp,}$ is about −5.3 kcal/mol (Eq. 3).

The observed heat capacity change may be described as a collective contribution of several factors, as shown in Eq. 6. At 298 K, the heat capacity change from the noncovalent interactions, ΔCp_{nc}, contributes about +6 to +7 cal/(mol·K) (29–31), and that of vibrating/stretching of covalent bonds is presumably negligible ($\Delta Cp_v = 0$). At pH 5.00, the protonation upon binding is minimized; ΔCp_p and ΔCp_{dp} approach zero. All of the above contribute only a small fraction of the observed intrinsic value, −234 ± 11 cal/(mol·K). The heat capacity change from SASA calculations (Table 3) accounts for 40–60% of this intrinsic value, indicating that the contribution from other factors, ΔCp_{ot}, is significantly large and negative.

At pH 6.25, the heat capacity change from deprotonation of the buffer, ΔCp_{dp} ($\Delta Cp_{dp\text{-}MES} = 3.8$ cal/(mol·K)) (26), contributes only 2 cal/mol·K to the observed value of −155 cal/(mol·K) (Fig. 5). Therefore, the difference in heat capacity change at pH 6.25 and pH 5.00 (+80 cal/(mol·K)) comes from the combined heat capacity changes, $\Delta Cp_p + \Delta Cp_{ot}$. Two factors that are not included specifically in the above analysis are the effect of the bound water and compound ''seesaw'' dynamics (17,18). In fact, it has been proposed that hydrogen bonds, solvent water, and polar groups are significant sources of the heat capacity change (34–36,56).

DISCUSSION

As noted above, a number of intercalators, as well as major groove binding aminoglycosides and proteins have linked-proton binding processes that are coupled to nucleic acid complex formation (1–3,5–10). The combination of spectroscopic and ITC methods used in analyzing the CGP DNA interactions shows clearly that AT-specific minor-groove binding compounds can also have proton uptake linked to complex formation. Titration results in Fig. 2 illustrate that CGP acquires an additional proton on the linker group when it binds to DNA at physiological conditions. This is expected, since the linker is an extended, conjugated guanidine analog. A large shift in pK_a value supports the linkage of protonation of the guanidine group to the binding, and shows that the binding energetics are enhanced when the linker is protonated. Experiments have shown that DNA grooves can be as much as two pH units lower than the surrounding solvent (12), and it is thus reasonable to have an increase of 2.7 units for the CGP linker. Protonation of the linker should also be enhanced by stronger hydrogen bonds with the thymine O2 atoms in the complex that are possible after protonation. Measurements of equilibrium constants at different salt concentrations (Fig. 6) show that the linker-protonated CGP has three electrostatic interactions with DNA. Besides enhancing H-bondings and providing additional electrostatic interactions that occur after protonation of the linker, the linker protonation also yields a symmetrical compound structure that contributes to symmetric ''seesaw'' H-bond dynamics, as previously described (17,18). Linker protonation thus seems to be a unique feature of the binding and interaction dynamics of the CGP complex.

Because of significant oligomer end effects, salt concentration can have a different influence on cationic interaction with DNA oligomers and polymers (57–60). Short oligomers have lower charge density and less counterion release per bound cation than polymers. The counterion density per phosphate at the ends of DNA oligomers is smaller than the average value of 0.88 Na^+ per phosphate of DNA polymers (49,52) and only approaches the polymer value several base pairs in from the ends. Thus, the use of $\phi = 0.88$ in the SPR binding studies under different pH values and salt concentrations yields the counterion release values of 2.38 and 2.26, which are lower than expected for a tricationic ligand. These values indicate that the counterion density per phosphate, $\phi = 0.88$, is an overestimated value for a short DNA hairpin, as expected. Back calculations predict a counterion density per phosphate of 0.68 ± 0.02 under these conditions for this oligomer and this is reasonable for the central region of short DNA hairpins. The value agrees well with predictions for other short oligomers (57,59).

It has been empirically shown that a number of factors, including the burial of nonpolar area contributes to negative heat capacity changes on biopolymer complex formation (29,43–45,47). This hydrophobic effect may contribute significantly to the observed negative heat capacity changes

for small molecule-DNA interactions (48,61). In addition, it has also been shown that trapping of a water molecule, as in the CGP complex, can lead to an additional negative heat capacity change (34). From the total buried area in the DNA minor groove on complex formation, it is clear that significant nonpolar surface of DNA is involved in the binding. The buried polar surface is considerably smaller and 80% of the total buried area is nonpolar. This is consistent with the prediction that hydrophobic interactions play a major role in complex formation. This may seem counterintuitive considering that the minor groove contains polar hydrogen acceptors such as O2 of thymine and N3 of adenine. However, a close inspection of the SASA of the DNA duplex (NMR structure, model 1) reveals that the majority of nonpolar buried area comes from the walls of the minor groove, where sugar rings and phosphorus atoms are predominant (Supplementary Materials, Fig. S3). This nonpolar characteristic of the minor-groove wall makes a significant contribution to the hydrophobic energetics upon interaction with minor-groove binders. This factor may need more attention in the design of minor-groove binding agents and optimizing binding affinities. The nonpolar characteristic of the minor groove is not entirely unexpected. It has been suggested from experiments with a minor-groove binding ligand that the minor groove in the AT sequence has strong nonpolar characteristics and a low dielectric constant (62). The low dielectric characteristic of the environment at the DNA grooves relative to bulk solvent has also been concluded for unbound grooves (63,64).

The intrinsic heat capacity change of the CGP/DNA complex (−234 cal/(mol·K)) at pH 5 is comparable to other small molecule/DNA complexes (65). By measuring the heat capacity at pH 5.00, where the free CGP linker is protonated, the heat capacity change associated with proton uptake is avoided. This effect could be large as previously noted in proteins (66). The calculated ΔCp_{SASA} accounts for only about half of the intrinsic value observed at pH 5.00. Therefore, the remaining portion must come from other factors, such as the bound water, polar groups, complex dynamics, or ion effects (ΔCp_{ot}) (32,33,56,67). It has been recently shown that a bound water molecule can contribute significantly to the overall heat capacity change (−18 cal/(mol·K)) (34). It has been also noted that the hydrophobic burial alone cannot fully account for the negative heat capacity change, especially when there is a significant conformation change (68). However, in this complex there is no significant conformation difference between the free and bound DNA.

In summary, the DNA binding properties of a linear minor-groove binding antitrypanosomal agent have been characterized. Upon complex formation at physiological conditions, spectroscopic and calorimetric studies indicate that the nitrogen-rich linker of the compound takes up a proton that leads to a total charge of +3. Biosensor binding studies with a short DNA hairpin indicate favorable electrostatic interactions of the protonated compound with DNA. Energetic decomposition (Supplementary Materials) suggests that the hydrophobic effect is one of the key players in driving the interaction, and other factors are also essential to yield the observed strong binding interaction of CGP with DNA.

SUPPLEMENTARY MATERIAL

An online supplement to this article can be found by visiting BJ Online at http://www.biophysj.org.

This work was supported by the National Institutes of Health through grants AI064200 and GM-61587. Instrumentation was purchased with partial support from the Georgia Research Alliance.

REFERENCES

1. Baker, B. M., and K. P. Murphy. 1996. Evaluation of linked protonation effects in protein binding reactions using isothermal titration calorimetry. *Biophys. J.* 71:2049–2055.
2. Petraccone, L., E. Erra, C. A. Mattia, V. Fedullo, G. Barone, and C. Giancola. 2004. Linkage of proton binding to the thermal dissociation of triple helix complex. *Biophys. Chem.* 110:73–81.
3. Dullweber, F., M. T. Stubbs, D. Musil, J. Sturzebecher, and G. Klebe. 2001. Factorising ligand affinity: a combined thermodynamic and crystallographic study of trypsin and thrombin inhibition. *J. Mol. Biol.* 313:593–614.
4. Li, W., P. Wu, T. Ohmichi, and N. Sugimoto. 2002. Characterization and thermodynamic properties of quadruplex/duplex competition. *FEBS Lett.* 526:77–81.
5. Jin, E., V. Katritch, W. K. Olson, M. Kharatisvili, R. Abagyan, and D. S. Pilch. 2000. Aminoglycoside binding in the major groove of duplex RNA: the thermodynamic and electrostatic forces that govern recognition. *J. Mol. Biol.* 298:95–110.
6. Kaul, M., and D. S. Pilch. 2002. Thermodynamics of aminoglycoside-rRNA recognition: the binding of neomycin-class aminoglycosides to the A site of 16S rRNA. *Biochemistry.* 41:7695–7706.
7. Kaul, M., C. M. Barbieri, J. E. Kerrigan, and D. S. Pilch. 2003. Coupling of drug protonation to the specific binding of aminoglycosides to the A site of 16 S rRNA: elucidation of the number of drug amino groups involved and their identities. *J. Mol. Biol.* 326:1373–1387.
8. Pilch, D. S., M. Kaul, C. M. Barbieri, and J. E. Kerrigan. 2003. Thermodynamics of aminoglycoside-rRNA recognition. *Biopolymers.* 70:58–79.
9. Renault, E., M. P. Fontaine-Aupart, F. Tfibel, M. Gardes-Albert, and E. Bisagni. 1997. Spectroscopic study of the interaction of pazelliptine with nucleic acids. *J. Photochem. Photobiol. B.* 40:218–227.
10. Sissi, C., S. Moro, S. Richter, B. Gatto, E. Menta, S. Spinelli, A. P. Krapcho, F. Zunino, and M. Palumbo. 2001. DNA-interactive anticancer aza-anthrapyrazoles: biophysical and biochemical studies relevant to the mechanism of action. *Mol. Pharmacol.* 59:96–103.
11. Lamm, G., and G. R. Pack. 1990. Acidic domains around nucleic acids. *Proc. Natl. Acad. Sci. USA.* 87:9033–9036.
12. Hanlon, S., L. Wong, and G. R. Pack. 1997. Proton equilibria in the minor groove of DNA. *Biophys. J.* 72:291–300.
13. Stanek, J., G. Caravatti, H. G. Capraro, P. Furet, H. Mett, P. Schneider, and U. Regenass. 1993. S-adenosylmethionine decarboxylase inhibitors: new aryl and heteroaryl analogues of methylglyoxal bis(guanylhydrazone). *J. Med. Chem.* 36:46–54.
14. Brun, R., Y. Buhler, U. Sandmeier, R. Kaminsky, C. J. Bacchi, D. Rattendi, S. Lane, S. L. Croft, D. Snowdon, V. Yardley, G. Caravatti, J. Frei, J. Stanek, and H. Mett. 1996. In vitro trypanocidal activities of new S-adenosylmethionine decarboxylase inhibitors. *Antimicrob. Agents Chemother.* 40:1442–1447.

15. Bacchi, C. J., R. Brun, S. L. Croft, K. Alicea, and Y. Buhler. 1996. In vivo trypanocidal activities of new S-adenosylmethionine decarboxylase inhibitors. *Antimicrob. Agents Chemother.* 40:1448–1453.

16. Johnson, R., J. C. Cubria, R. M. Reguera, R. Balana-Fouce, and D. Ordonez. 1998. Interaction of cationic diamidines with *Leishmania infantum* DNA. *Biol. Chem.* 379:925–930.

17. Nguyen, B., M. P. Lee, D. Hamelberg, A. Joubert, C. Bailly, R. Brun, S. Neidle, and W. D. Wilson. 2002. Strong binding in the DNA minor groove by an aromatic diamidine with a shape that does not match the curvature of the groove. *J. Am. Chem. Soc.* 124:13680–13681.

18. Nguyen, B., D. Hamelberg, C. Bailly, P. Colson, J. Stanek, R. Brun, S. Neidle, and W. D. Wilson. 2004. Characterization of a novel DNA minor-groove complex. *Biophys. J.* 86:1028–1041.

19. Cantor, C. R., and I. Tinoco, Jr. 1965. Absorption and optical rotatory dispersion of seven trinucleoside diphosphates. *J. Mol. Biol.* 13: 65–77.

20. Cantor, C. R., M. M. Warshaw, and H. Shapiro. 1970. Oligonucleotide interactions. 3. Circular dichroism studies of the conformation of deoxyoligonucleotides. *Biopolymers.* 9:1059–1077.

21. Fasman, G. D. 1975. Handbook of Biochemistry and Molecular Biology. Nucleic Acids. G. Fasman, editor. CRC Press, Cleveland, OH. 589 p.

22. Lacy, E. R., B. Nguyen, M. Le, K. K. Cox, C. O'Hare, J. A. Hartley, M. Lee, and W. D. Wilson. 2004. Energetic basis for selective recognition of T*G mismatched base pairs in DNA by imidazole-rich polyamides. *Nucleic Acids Res.* 32:2000–2007.

23. Briggner, L. E., and I. Wadso. 1991. Test and calibration processes for microcalorimeters, with special reference to heat conduction instruments used with aqueous systems. *J. Biochem. Biophys. Methods.* 22: 101–118.

24. Wiseman, T., S. Williston, J. F. Brandts, and L. N. Lin. 1989. Rapid measurement of binding constants and heats of binding using a new titration calorimeter. *Anal. Biochem.* 179:131–137.

25. Horn, J. R., D. Russell, E. A. Lewis, and K. P. Murphy. 2001. Van't Hoff and calorimetric enthalpies from isothermal titration calorimetry: are there significant discrepancies? *Biochemistry.* 40:1774–1778.

26. Fukada, H., and K. Takahashi. 1998. Enthalpy and heat capacity changes for the proton dissociation of various buffer components in 0.1 M potassium chloride. *Proteins.* 33:159–166.

27. Davis, T. M., and W. D. Wilson. 2000. Determination of the refractive index increments of small molecules for correction of surface plasmon resonance data. *Anal. Biochem.* 284:348–353.

28. Makhatadze, G. I., and P. L. Privalov. 1995. Energetics of protein structure. *Adv. Protein Chem.* 47:307–425.

29. Murphy, K. P., and E. Freire. 1992. Thermodynamics of structural stability and cooperative folding behavior in proteins. *Adv. Protein Chem.* 43:313–361.

30. Gomez, J., V. J. Hilser, D. Xie, and E. Freire. 1995. The heat capacity of proteins. *Proteins.* 22:404–412.

31. Gomez, J., and E. Freire. 1995. Thermodynamic mapping of the inhibitor site of the aspartic protease endothiapepsin. *J. Mol. Biol.* 252: 337–350.

32. Morton, C. J., and J. E. Ladbury. 1996. Water-mediated protein-DNA interactions: the relationship of thermodynamics to structural detail. *Protein Sci.* 5:2115–2118.

33. Bergqvist, S., M. A. Williams, R. O'Brien, and J. E. Ladbury. 2004. Heat capacity effects of water molecules and ions at a protein-DNA interface. *J. Mol. Biol.* 336:829–842.

34. Cooper, A. 2005. Heat capacity effects in protein folding and ligand binding: a re-evaluation of the role of water in biomolecular thermodynamics. *Biophys. Chem.* 115:89–97.

35. Cooper, A. 2000. Heat capacity of hydrogen-bonded networks: an alternative view of protein folding thermodynamics. *Biophys. Chem.* 85:25–39.

36. Cooper, A., C. M. Johnson, J. H. Lakey, and M. Nollmann. 2001. Heat does not come in different colours: entropy-enthalpy compensation, free energy windows, quantum confinement, pressure perturbation calorimetry, solvation and the multiple causes of heat capacity effects in biomolecular interactions. *Biophys. Chem.* 93:215–230.

37. Berman, H. M., W. K. Olson, D. L. Beveridge, J. Westbrook, A. Gelbin, T. Demeny, S. H. Hsieh, A. R. Srinivasan, and B. Schneider. 1992. The nucleic acid database. A comprehensive relational database of three-dimensional structures of nucleic acids. *Biophys. J.* 63:751–759.

38. Nicholls, A., K. A. Sharp, and B. Honig. 1991. Protein folding and association: insights from the interfacial and thermodynamic properties of hydrocarbons. *Proteins.* 11:281–296.

39. Cornell, W. D., P. Cieplak, C. I. Bayly, I. R. Gould, K. M. Merz, Jr., D. M. Ferguson, D. C. Spellmeyer, T. Fox, J. W. Caldwell, and P. A. Kollman. 1995. A second generation force field for the simulation of proteins, nucleic acids, and organic molecules. *J. Am. Chem. Soc.* 117: 5179–5197.

40. Tjandra, N., S.-i. Tate, A. Ono, M. Kainosho, and A. Bax. 2000. The NMR structure of a DNA dodecamer in an aqueous dilute liquid crystalline phase. *J. Am. Chem. Soc.* 122:6190–6200.

41. Shui, X., L. McFail-Isom, G. G. Hu, and L. D. Williams. 1998. The B-DNA dodecamer at high resolution reveals a spine of water on sodium. *Biochemistry.* 37:8341–8355.

42. Spolar, R. S., J. H. Ha, and M. T. Record, Jr. 1989. Hydrophobic effect in protein folding and other noncovalent processes involving proteins. *Proc. Natl. Acad. Sci. USA.* 86:8382–8385.

43. Livingstone, J. R., R. S. Spolar, and M. T. Record, Jr. 1991. Contribution to the thermodynamics of protein folding from the reduction in water-accessible nonpolar surface area. *Biochemistry.* 30:4237–4244.

44. Spolar, R. S., J. R. Livingstone, and M. T. Record, Jr. 1992. Use of liquid hydrocarbon and amide transfer data to estimate contributions to thermodynamic functions of protein folding from the removal of nonpolar and polar surface from water. *Biochemistry.* 31:3947–3955.

45. Spolar, R. S., and M. T. Record, Jr. 1994. Coupling of local folding to site-specific binding of proteins to DNA. *Science.* 263:777–784.

46. Habermann, S. M., and K. P. Murphy. 1996. Energetics of hydrogen bonding in proteins: a model compound study. *Protein Sci.* 5:1229–1239.

47. Murphy, K. P., V. Bhakuni, D. Xie, and E. Freire. 1992. Molecular basis of co-operativity in protein folding. III. Structural identification of cooperative folding units and folding intermediates. *J. Mol. Biol.* 227:293–306.

48. Ren, J., T. C. Jenkins, and J. B. Chaires. 2000. Energetics of DNA intercalation reactions. *Biochemistry.* 39:8439–8447.

49. Record, M. T., Jr., C. F. Anderson, and T. M. Lohman. 1978. Thermodynamic analysis of ion effects on the binding and conformational equilibria of proteins and nucleic acids: the roles of ion association or release, screening, and ion effects on water activity. *Q. Rev. Biophys.* 11:103–178.

50. Lorz, E., and R. Baltzly. 1949. N,N-disubstituted amidines. II. Benzamidines. The Effect of Substitution on Basicity. *J. Am. Chem. Soc.* 71:3992–3994.

51. Patai, S., and Z. Rappoport. 1991. The Chemistry of Amidines and Imidates, Vol. 2. John Wiley & Sons, New York.

52. Manning, G. S. 1978. The molecular theory of polyelectrolyte solutions with applications to the electrostatic properties of polynucleotides. *Q. Rev. Biophys.* 11:179–246.

53. Cheatham 3rd, T. E. 2004. Simulation and modeling of nucleic acid structure, dynamics and interactions. *Curr. Opin. Struct. Biol.* 14:360–367.

54. Cheatham 3rd, T. E., and P. A. Kollman. 2000. Molecular dynamics simulation of nucleic acids. *Annu. Rev. Phys. Chem.* 51:435–471.

55. Cheatham 3rd, T. E., and M. A. Young. 2000. Molecular dynamics simulation of nucleic acids: successes, limitations, and promise. *Biopolymers.* 56:232–256.

56. Chalikian, T. V. 2003. Hydrophobic tendencies of polar groups as a major force in molecular recognition. *Biopolymers.* 70:492–496.

57. Olmsted, M. C., J. P. Bond, C. F. Anderson, and M. T. Record, Jr. 1995. Grand canonical Monte Carlo molecular and thermodynamic predictions of ion effects on binding of an oligocation (L8+) to the center of DNA oligomers. *Biophys. J.* 68:634–647.

58. Zhang, W., J. P. Bond, C. F. Anderson, T. M. Lohman, and M. T. Record, Jr. 1996. Large electrostatic differences in the binding thermodynamics of a cationic peptide to oligomeric and polymeric DNA. *Proc. Natl. Acad. Sci. USA.* 93:2511–2516.

59. Zhang, W., H. Ni, M. W. Capp, C. F. Anderson, T. M. Lohman, and M. T. Record, Jr. 1999. The importance of Coulombic end effects: experimental characterization of the effects of oligonucleotide flanking charges on the strength and salt dependence of oligocation (L8+) binding to single-stranded DNA oligomers. *Biophys. J.* 76:1008–1017.

60. Shkel, I. A., and M. T. Record, Jr. 2004. Effect of the number of nucleic acid oligomer charges on the salt dependence of stability (ΔG 37°) and melting temperature (T_m): NLPB analysis of experimental data. *Biochemistry.* 43:7090–7101.

61. Mazur, S., F. A. Tanious, D. Ding, A. Kumar, D. W. Boykin, I. J. Simpson, S. Neidle, and W. D. Wilson. 2000. A thermodynamic and structural analysis of DNA minor-groove complex formation. *J. Mol. Biol.* 300:321–337.

62. Jin, R., and K. J. Breslauer. 1988. Characterization of the minor groove environment in a drug-DNA complex: bisbenzimide bound to the poly [d(AT)].poly[d(AT)]duplex. *Proc. Natl. Acad. Sci. USA.* 85:8939–8942.

63. Lamm, G., and G. R. Pack. 1997. Local dielectric constants and Poisson-Boltzmann calculations of DNA counterion distributions. *Int. J. Quantum Chem.* 65:1087–1093.

64. Lamm, G., and G. R. Pack. 1997. Calculation of dielectric constants near polyelectrolytes in solution. *J. Phys. Chem. B.* 101:959–965.

65. Haq, I. 2002. Thermodynamics of drug-DNA interactions. *Arch. Biochem. Biophys.* 403:1–15.

66. Kozlov, A. G., and T. M. Lohman. 2000. Large contributions of coupled protonation equilibria to the observed enthalpy and heat capacity changes for ssDNA binding to *Escherichia coli* SSB protein. *Proteins.* 4:8–22.

67. Sturtevant, J. M. 1977. Heat capacity and entropy changes in processes involving proteins. *Proc. Natl. Acad. Sci. USA.* 74:2236–2240.

68. Barbieri, C. M., A. R. Srinivasan, and D. S. Pilch. 2004. Deciphering the origins of observed heat capacity changes for aminoglycoside binding to prokaryotic and eukaryotic ribosomal RNA a-sites: a calorimetric, computational, and osmotic stress study. *J. Am. Chem. Soc.* 126:14380–14388.